# Coulomb excitation of $^{104}$Sn and the strength of the $^{100}$Sn shell closure

G. Guastalla,[1] D.D. DiJulio,[2] M. Górska,[3] J. Cederkäll,[2] P. Boutachkov,[1,3] P. Golubev,[2] S. Pietri,[3] H. Grawe,[3] F. Nowacki,[4] K. Sieja,[4] A. Algora,[5] F. Ameil,[3] T. Arici,[6,3] A. Atac,[7] M. A. Bentley,[8] A. Blazhev,[9] D. Bloor,[8] S. Brambilla,[10] N. Braun,[9] F. Camera,[10] C. Domingo Pardo,[11] A. Estrade,[3] F. Farinon,[3] J. Gerl,[3] N. Goel,[3,1] J. Grębosz,[12] T. Habermann,[3,13] R. Hoischen,[2] K. Jansson,[2] J. Jolie,[9] A. Jungclaus,[14] I. Kojouharov,[3] R. Knoebel,[3] R. Kumar,[15] J. Kurcewicz,[16] N. Kurz,[3] N. Lalović,[3] E. Merchan,[1,3] K. Moschner,[9] F. Naqvi,[3,9] B. S. Nara Singh,[8] J. Nyberg,[17] C. Nociforo,[3] A. Obertelli,[18] M. Pfützner,[3,19] N.Pietralla,[1] Z. Podolyák,[20] A. Prochazka,[3] D. Ralet,[1,3] P. Reiter,[9] D. Rudolph,[2] H. Schaffner,[3] F. Schirru,[20] L. Scruton,[8] T. Swaleh,[2] J. Taprogge,[9,21] R. Wadsworth,[8] N. Warr,[9] H. Weick,[3] A. Wendt,[9] O. Wieland,[10] J.S. Winfield,[3] and H. J. Wollersheim[3]

[1] *Institut für Kernphysik, Technische Universität Darmstadt, Darmstadt, Germany*
[2] *Department of Physics, Lund University, Lund, Sweden*
[3] *Helmholtzzentrum für Schwerionenforschung GmbH (GSI), Darmstadt, Germany*
[4] *IPHC, IN2P3-CNRS et Université de Strasbourg, Strasbourg, France*
[5] *IFIC (CSIS-Univ. Valencia) Valencia, Spain*
[6] *Institute of Science, Istanbul University, Turkey*
[7] *Department of Physics, Ankara University, Ankara, Turkey*
[8] *Department of Physics, University of York, York, United Kingdom*
[9] *Institut für Kernphysik, Universität zu Köln, Köln, Germany*
[10] *Dipartimento di Fisica, Università di Milano, and INFN Sezione Milano, Milano, Italy*
[11] *Instituto de Fisica Corpuscular Apdo. Correos, Valencia, Spain*
[12] *The Institute of Nuclear Physics PAN, Kraków, Poland*
[13] *Department of Physics, Goethe University, Frankfurt am Main, Germany*
[14] *Instituto de Estructura de la Materia, CSIC, Madrid, Spain*
[15] *Inter-University Acceleration Center, New Dehli, India*
[16] *The Institute of Experimental Physics, Warsaw, Poland*
[17] *Department of Physics and Astronomy, Uppsala University, Uppsala, Sweden*
[18] *CEA, Centre de Saclay, IRFU/Service de Physique Nucléaire, Gif-sur-Yvette, France*
[19] *Faculty of Physics, University of Warsaw, Warsaw, Poland*
[20] *Department of Physics, University of Surrey, Guildford, United Kingdom*
[21] *Departamento de Física Teórica, Universidad Autónoma de Madrid, Madrid, Spain*

(Dated: January 16, 2013)

A measurement of the reduced transition probability for the excitation of the ground state to the first $2^+$ state in $^{104}$Sn has been performed using relativistic Coulomb excitation at GSI. $^{104}$Sn is the lightest isotope in the Sn chain for which this quantity has been measured. It is also the heaviest neutron-deficient Sn isotope for which a large scale shell model calculation can be performed without significant truncation. The result is therefore a key point in the discussion of the evolution of nuclear structure in the proximity of the doubly magic nucleus $^{100}$Sn. The value $B(E2; 0^+ \to 2^+) = 0.10(4)$ $e^2$b$^2$ is significantly lower than earlier results for $^{106}$Sn and heavier isotopes. The result is well reproduced by shell model predictions and therefore indicates a robust $N = Z =$50 shell closure.

The properties of many composite quantum objects that represent building blocks of matter, such as hadrons, atomic nuclei, atoms, and molecules are governed by energy gaps between quantum states which originate in the forces between their fermionic constituents. In the case of atomic nuclei, the energy gaps manifest themselves by the existence of specific stable isotopes. These include e.g. the double shell-closure nuclei $^4$He, $^{16}$O, $^{40,48}$Ca, and $^{208}$Pb, which are particularly robust against particle separation and intrinsic excitation. The $\beta$-unstable isotopes $^{56}$Ni, $^{78}$Ni, and $^{100,132}$Sn are also expected to correspond to double shell closures. However, data for $^{78}$Ni and $^{100}$Sn are scarce due to their exotic neutron-to-proton ratios. Therefore, there is considerable interest in finding more proof for the magicity of these isotopes. In addition, the single particle energies relative to $^{100}$Sn are largely unknown experimentally. Data is limited to the energy splitting between the two lowest-energy orbitals [1, 2] while extrapolations from nearby nuclei are available with a typical uncertainty of a few hundred keV for the orbitals of higher energy [3]. Since $^{100}$Sn is predicted to be a doubly-magic nucleus it would provide an approximately inert core on top of which simple excitations can be formed by adding few particles or holes. For this reason, it presents a unique testing ground for fundamental nuclear models. Another cause for increased interest in nuclear structure in this region comes from the the *rp*-process of nuclear synthesis [4]. It has been concluded recently that this reaction sequence comes to an end near $^{100}$Sn [4]. In addition, $^{100}$Sn itself is expected to be the heaviest self-conjugate doubly-magic nucleus. Therefore, it provides the core for the heaviest odd-odd

$N = Z$ nuclei for which Coulomb corrections for superallowed $\beta$-decays can be extracted. This is of importance for the unitary test of the CKM matrix via the measurement of its $V_{ud}$ element [5].

The size of the $N = 50$ neutron shell gap has so far been inferred from core excited states of lighter neighbouring nuclei [6, 7]. Similar conclusions have been drawn for the $Z = 50$ proton shell closure based on the distribution of the Gamow-Teller (GT) decay strength of $^{100}$Sn [8]. Here, the new generation of radioactive ion beam facilities have recently started to provide spectroscopic access to selected states as well as to electroweak transition rates. A direct measure of the stability against quadrupole excitations and therefore an alternative signature for the robustness of a shell closure is provided by the $E2$ excitation strength, as quantified by the $B(E2; 0^+ \rightarrow 2_1^+)$ value. As $^{100}$Sn is not yet accessible for such measurements, a series of experiments have been performed for neutron-deficient Sn isotopes over the past few years [9–12]. These data show excessive experimental $B(E2)$ strength compared to shell model calculations below neutron number $N = 64$. The results do not exclude a constant or even increasing collectivity below $^{106}$Sn. Larger than expected reduced transition probabilities have also been observed recently in the neutron deficient odd-mass Sn isotopes [13, 14]. In combination with the observations in the lightest Te [15] and Xe [16] isotopes, these measurements may call into question the assumption of $^{100}$Sn as an inert shell-model core.

It is unclear at present whether the deviations between shell model calculations and experiments are due to truncation imposed by computational limits or due to deficiencies in the effective interactions [17]. A measurement of an even-even isotope closer to $^{100}$Sn is desirable since that means a smaller and more tractable model space can be used for the calculations. It is the purpose of the present paper to report on the first measurement of the $E2$ excitation strength for $^{104}$Sn. The new data indicate a reduction of the $B(E2; 0^+ \rightarrow 2_1^+)$ value with decreasing neutron number. The result is in line with large scale shell model (LSSM) calculations that show a decrease in the $E2$ strength with decreasing neutron number exhibiting a local minimum for $^{102}$Sn. This minimum can be understood as arising from the robustness of the $Z = 50$ proton shell closure together with the blocking of the $E2$ strength by valence neutrons.

The experiment was performed at the Helmholtzzentrum für Schwerionenforschung (GSI) using the PreSPEC setup. The $^{104}$Sn beam was produced by nuclear fragmentation of a $^{124}$Xe beam at 793 MeV/$u$ which impinged on a 4 g/cm$^2$ $^9$Be target. The beam was separated in the FRagment Separator (FRS) [18] using the magnetic rigidity B$\rho$ and the energy loss in a 2.0 g/cm$^2$ and a 2.4 g/cm$^2$ thick degrader at its first and middle focal planes, respectively. Identification and event-by-event tracking of the ions were provided by detectors placed at the middle and final focal planes of the FRS. The identification plot for the experiment is shown in Fig. 1. The energy of the $^{104}$Sn ions at the secondary target was $\sim$140 MeV/$u$ as calculated by LISE++ [19] for the FRS.

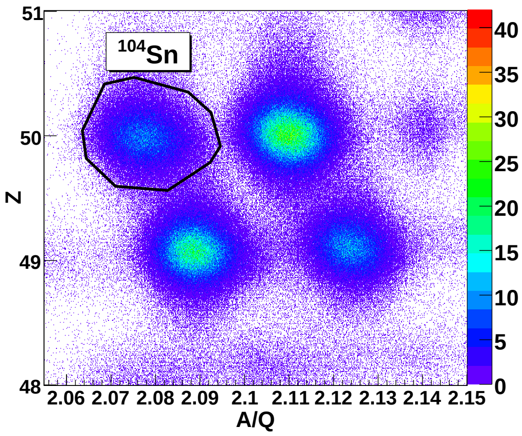


FIG. 1. Identification plot for the $^{104}$Sn secondary beam. The x-axis is the $A/Q$, where $A$ is the mass and $Q$ is the charge of the nuclei, obtained from a time of flight measurement, and the y-axis is the nuclear charge Z, obtained from a $\Delta E$ measurement.

The secondary beam was focused on a $^{197}$Au target with a thickness of 386 mg/cm$^2$ positioned at the final focal plane of the FRS. The spatial distribution of the ions at the target location was measured event by event by a Double Sided Silicon Strip Detector (DSSSD). The emitted $\gamma$ rays were detected by the RISING array, which comprised 15 EUROBALL Cluster detectors, placed at forward angles in three rings at 16°, 33° and 36° [20–22]. The $\gamma$ rays were recorded event by event in coincidence with particles hitting a plastic scintillator placed in front of the secondary target. The Lund York Cologne CAlorimeter (LYCCA) [23–25] was used to identify the ions after the target. LYCCA provides information on the nuclear charges, velocities, and scattering angles of the reaction products. The $\Delta E - E$ plot for ions after the $^{197}$Au target is shown in Fig. 2.

The analysis was optimized in order to enhance the peak-to-background ratio for the $2^+ \rightarrow 0^+$ transition. The ions were selected using the same proton number for incoming and outgoing particles at the secondary target. A scattering angle range of 15-40 mrad was chosen in order to select relativistic Coulomb excitation events and to reduce the contribution from nuclear reactions. A total of $2.7 \times 10^7$ $^{104}$Sn ions were identified. The prompt $\gamma$-ray coincidence window was set to 15 ns. The velocities of the ions after the target were extracted event by event. The velocity distribution obtained from the LISE++ simulations was used as a guide for the centroid position of the experimental distribution. The Doppler correction was calculated event by event from the ion scattering angles

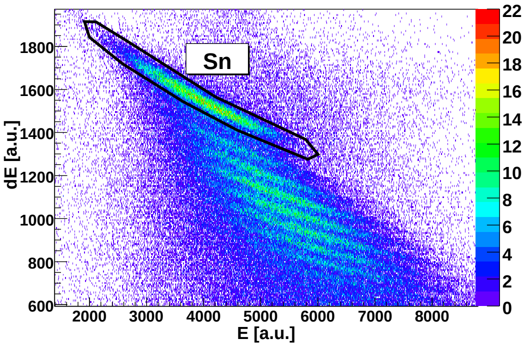


FIG. 2. $\Delta E - E$ plot for the ions after the $^{197}$Au target. The x-axis is the total energy deposited in the LYCCA CsI, and the y-axis is the energy loss in the LYCCA DSSSD.

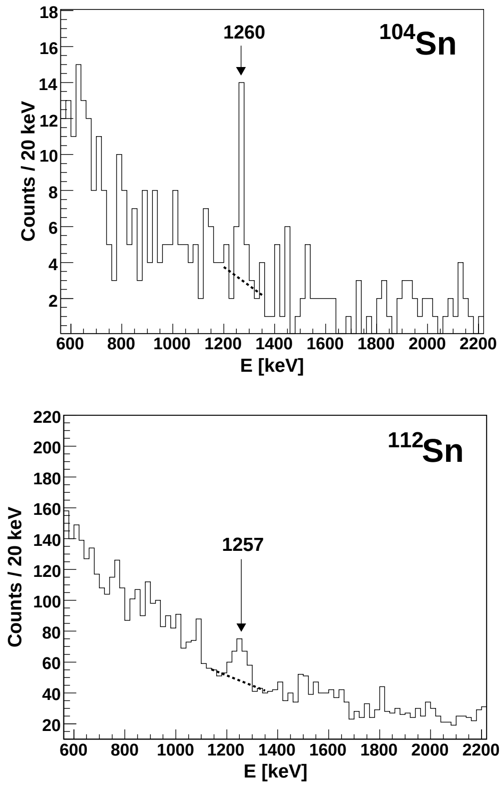


FIG. 3. Doppler corrected energy spectra for $^{104}$Sn (upper panel), and for $^{112}$Sn (lower panel). The $E2$ transition of interest is visible at 1260 keV and 1257 keV for $^{104}$Sn and $^{112}$Sn, respectively. The dashed line represents an extrapolation of the background used in the analysis.

and the emission angles of the $\gamma$ rays. The resulting spectrum is shown in the top panel of Fig. 3. The $\gamma$ ray of interest is at 1260 keV [26, 27].

A calibration measurement was carried out with $^{112}$Sn, under conditions similar to the $^{104}$Sn case, in order to use its known $B(E2; 0^+ \rightarrow 2^+)$ value for normalization. The energy of the $^{124}$Xe beam was 700 MeV/$u$. A total of 6.5$\times$10$^7$ $^{112}$Sn ions were identified with an energy of $\sim$140 MeV/$u$. The Doppler corrected spectrum for $^{112}$Sn is shown in the lower panel of Fig. 3. In view of the small difference between the transition energies in $^{104}$Sn and $^{112}$Sn no efficiency correction was applied in the analysis. The width of the peak in the lower panel can be inferred from the short lifetime of the $2^+$ state (below $\sim$1 ps [28, 29]). This leads to a significant number of deexcitation gamma rays being emitted in the target. The shape of the background is similar in both cases but the background level is significantly higher for $^{112}$Sn. This is a result of the higher instantaneous rate which increases the random coincidence probability. The final spectra contained 16(5) and 95(24) counts for the $2^+ \rightarrow 0^+$ transitions in $^{104}$Sn and $^{112}$Sn, respectively. The reduced transition probability for $^{104}$Sn was extracted from the proportionality of the Coulomb excitation cross section and the photon yield taking into account the number of detected ions. The following expression can be applied in this situation:

$$B(E2\uparrow)_{104} = B(E2\uparrow)_{112} \times \frac{N_\gamma^{104}}{N_\gamma^{112}} \times \frac{N_{part}^{112}}{N_{part}^{104}} \times 0.96.$$

The quantity $B(E2\uparrow)$ is the $B(E2; 0^+ \rightarrow 2_1^+)$ value for the two cases. $N_\gamma^{104}$ and $N_\gamma^{112}$ are the number of counts in the two $\gamma$-ray peaks and $N_{part}^{104}$ and $N_{part}^{112}$ are the number of incoming beam particles for the two cases. The factor 0.96 originates in a correction for different impact parameters for $^{104,112}$Sn ions as calculated with the code DWEIKO [30]. A reference value of $B(E2) = 0.242(8)$ $e^2$b$^2$ for $^{112}$Sn was used for normalization as measured in a sub-barrier Coulomb excitation experiment [28]. An approximately 20% lower value would result if a recent value based on a lifetime measurement is instead used for normalization [29]. The $B(E2)$ value extracted for $^{104}$Sn is $B(E2; 0^+ \rightarrow 2^+) = 0.10(4)$ $e^2$b$^2$ or $B(E2\downarrow) = 6.9(30)$ W.u. The new result is three standard deviations smaller than the average of the $^{106-114}$Sn values, which is indicated by the shaded bar in Fig. 4. It is also two standard deviations smaller than the $^{106}$Sn data [11, 12]. This result clearly establishes a decreasing trend of $B(E2)$ values towards $^{100}$Sn.

LSSM calculations were carried out in the *gds* model space using a $^{80}$Zr core in order to investigate the underlying microscopic structure. For the $N$=4 harmonic oscillator shell, the present truncation limit is $6p6h$ ($t$=6) in the *gds* space, which reaches convergence for excitation energies and transition strengths for $^{100}$Sn. The effective interaction used in the calculations was derived from the realistic CD-Bonn potential [31] and adapted to the model space by many-body perturbation theory techniques assuming a hypothetical $^{80}$Zr core [32]. The monopole term was tuned to reproduce the measured single particle/single hole energies around $^{90}$Zr and their extrapolated values for $^{100}$Sn [6, 7]. The calculations were performed with the shell-model codes ANTOINE and NATHAN [33, 34] at the $t$=6 level for $^{100}$Sn, $t$=5 for $^{102}$Sn, and $t$=4 for $^{104}$Sn. An alternative truncation scheme was employed for $^{100-106}$Sn allowing $t_\pi$=4 for protons and $t_\nu$=2 for neutrons along with seniority truncation for neutrons together with the interaction given in [9]. The results for the two cases agree well for the overlapping nuclei. Therefore only the ones obtained in the latter approach are shown as the red full line in Fig. 4. The results using a $^{90}$Zr core, as described in Ref. [9], are shown as a blue dashed line. The effect of the additional neutron degrees of freedom are evident in the overlapping region. Good agreement is obtained for $^{104}$Sn and for the increasing $B(E2)$ trend towards the heavier Sn isotopes. A common polarization charge of 0.5$e$ for protons and neutrons was used. The recently discussed [35–39] isovector dependence of $E2$ polarization charges due to coupling to the giant quadrupole resonance outside the model space will lead to at most a marginal increase of $B(E2)$ values since at $N \sim Z$ the isoscalar part dominates. However, the agreement with the global $^{100-132}$Sn trend, i.e. the asymmetry with with respect to the middle of the $N = 50 - 82$ neutron shell [9–11], is improved by this effect.

The notion that doubly-magic nuclei exhibit a minimum in $B(E2; 2^+ \rightarrow 0^+)$ values in an isotopic chain is strictly true only for spin-orbit (SO) closed harmonic oscillator shells. Among these are $^{16}$O, $^{40}$Ca and the partially SO-closed $^{48}$Ca, $^{68}$Ni and $^{90}$Zr. In these nuclei spin and quadrupole $ph$-excitation modes are suppressed by the parity change to the subsequent shell. On the other hand, SO-open shell closures allow parity-conserving spin-flip transitions between SO-partner orbitals as well as $\Delta j$=$\Delta l$=2 stretched $E2$ $ph$ excitations which gives rise to an enhanced spin (GT) and quadrupole ($E2$) response of the nucleus. The increase of the $B(E2)$ value, calculated for $^{100}$Sn, is a signature of the purity of its ground state. The recent measurement of the GT strength implies that it consists of ~80% of the closed-shell configuration while the first excited $2^+$ state is dominated by $\Delta l = 2$ $ph$ excitations. Excitations of $ph$ configurations are partially blocked when adding valence neutrons in the $N = 50 - 82$ shell which dominate the ground state configuration. This leads to the local minimum for the $B(E2)$ strength at $^{102}$Sn. This reduction of the $B(E2)$ value from the doubly-magic nucleus to its neighboring semi-magic even-even isotope is at variance with the observation in the $N$=3, $fp$ shell for the Ni isotopes and for the $N = 50$ isotones above $Z = 28$ [17].

In $^{56}$Ni, which is the lighter doubly-magic spin-orbit open neighbor of $^{100}$Sn, core excitations amount to about 50% of the ground state wave function according to shell-model calculations [40, 41]. In this case, parity-conserving $\Delta j$=$\Delta l$=2 stretched $E2$ $ph$ excitations give rise to an enhanced quadrupole response of the nucleus, which persists when valence neutrons are added. The calculated reduction of the $B(E2)$ value from $^{100}$Sn to $^{104}$Sn corresponds to a similar effect near the doubly-magic nuclei $^{132}$Sn [42, 43] and $^{208}$Pb [43, 44]. It corroborates the robust $N = Z = 50$ shell closure inferred from the strength of the $\beta^+$/EC-decay of $^{100}$Sn [8]. Further verification of the shell-model calculations from $^{100-104}$Sn provide an interesting challenge for future experiments.

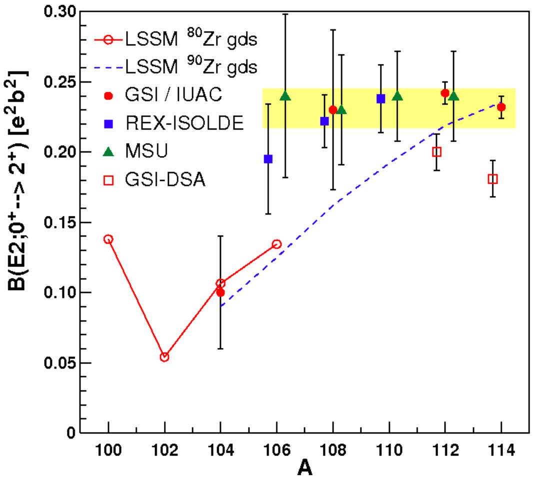


FIG. 4. Experimental $B(E2; 0^+ \rightarrow 2^+)$ values for $^{104-114}$Sn from Coulomb excitation and LSSM results for $^{100-114}$Sn. The data were measured at REX-ISOLDE [10, 12], MSU [11], GSI [9] and in the present work. The $^{112}$Sn reference point is taken from [28], the $^{114}$Sn value from [45] and compared to data from Doppler lineshape analysis [29]. LSSM results with a $^{80}$Zr core are shown for truncation $t_\pi$=4, $t_\nu$=2 and seniority truncation for neutrons in $^{100-106}$Sn (full red line). LSSM calculations for $^{102-114}$Sn with a $^{90}$Zr core (dashed blue line) are taken from Ref. [9]. The shaded bar represents the averaged value for $^{106-114}$Sn Coulomb excitation data.

In summary, the $B(E2; 0^+ \rightarrow 2^+)$ value for $^{104}$Sn has been measured by relativistic Coulomb excitation. The result establishes a significant reduction of the $B(E2)$ strength from $^{106}$Sn to $^{104}$Sn and a downward trend towards $^{102}$Sn. It implies enhanced stability of the $N = Z = 50$ shell closure against $ph$-excited quadrupole modes. This signature is in line with the heavier doubly-magic partners $^{132}$Sn and $^{208}$Pb but deviates from the behavior of its lighter $N = Z$ spin-orbit open companion $^{56}$Ni. LSSM calculations in the $gds$ model space, without significant truncation as described above, account for the $^{104}$Sn value within experimental uncertainties. Whether the excessive $B(E2)$ strength observed between $N = 56$ and 64 is solely due to polarization charge, to the effective interaction and/or to a neutron sub-shell effect remains an open question at this stage. Future LSSM calculations treating excitation energies, $B(E2)$ values and binding energies on the same footing in combination with new high precision measurements may provide a solution for this issue.

This work was supported by the Helmholtz International Center for FAIR (HIC for FAIR) within the

LOEWE program by the State of Hesse, the BMBF under grant No. 05P12RDFN8, and the Swedish Research Council through contract No. 2009-3939. A.J. would like to thank the "Spanish Ministerio de Ciencia e Innovacin for finicial support under contract number FPA2011-29854-C04. A.B. acknowledges the support of the German BMBF under contract No. 06KY9135I.

[1] D. Seweryniak et al., Phys. Rev. Lett. **99**, 022504 (2007).
[2] I. G. Darby et al., Phys. Rev. Lett. **105**, 162502 (2010).
[3] H. Grawe, K. Langanke, and G. Martinez-Pinedo, Rep. Prog. Phys. **70**, 1525 (2007).
[4] H. Schatz et al., Phys. Rev. Lett. **86**, 3471 (2001).
[5] J. C. Hardy and I. S. Towner, Phys. Rev. C **79**, 055502 (2009).
[6] A. Blazhev et al., Phys. Rev. **C69**, 064304 (2004).
[7] P. Boutachkov et al., Phys. Rev. **C84**, 044311 (2011).
[8] C. Hinke et al., Nature **486**, 341 (2012).
[9] A. Banu et al., Phys. Rev. **C72**, 061305 (2005).
[10] J. Cederkäll et al., Phys. Rev. Lett. **98**, 172501 (2007).
[11] C. Vaman et al., Phys. Rev. Lett. **99**, 162501 (2007).
[12] A. Ekström et al., Phys. Rev. Lett. **101**, 012502 (2008).
[13] D. D. DiJulio et al., Eur. Phys. J A **48**, 105 (2012).
[14] D. D. DiJulio et al., Phys. Rev. C **86**, 031302(R) (2012).
[15] B. Hadinia et al., Phys. Rev. **C 72**, 041303 (2005).
[16] M. Sandzelius et al., Phys. Rev. Lett. **99**, 022501 (2007).
[17] T. Faestermann, M. Górska, and H. Grawe, Progr. Part. Nucl. Phys. **68**, 85 (2013).
[18] H. Geissel et al., Nucl. Instrum. Methods Phys. Res. **B70**, 286 (1992).
[19] O. B. Tarasov and D. Bazin, Nucl. Instrum. Methods Phys. Res. **B266**, 4657 (2008).
[20] H. J. Wollersheim et al., Nucl. Instrum. Methods Phys. Res. **A537**, 637 (2005).
[21] J. Simpson, Z. Phys. **A358**, 139 (1997).
[22] J. Eberth et al., Nucl. Instrum. Methods Phys. Res. **A369**, 135 (1996).
[23] D. Rudolph et al., "Lycca technical design report, 2008," `http://www.nuclear.lu.se/english/research/basic_nuclear_physics/nustar/lycca`.
[24] R. Hoischen et al., Nucl. Instrum. Methods Phys.Res. **A 654**, 354 (2011).
[25] M. J. Taylor et al., Nucl. Instrum. Methods Phys. Res. **A 606**, 589 (2009).
[26] R. Schubart et al., Z. Phys. **A 340**, 109 (1991).
[27] M. Górska et al., Phys. Rev. **C 58**, 108 (1998).
[28] R. Kumar et al., Phys. Rev. C **81**, 024306 (2010).
[29] A. Jungclaus et al., Phys. Lett. **B 695**, 110 (2007).
[30] C. A. Bertulani, C. M. Campbell, and T. Glasmacher, Comput. Phys. Commun. **152**, 317 (2003).
[31] R. Machleidt, Phys. Rev. **C63**, 024001 (2001).
[32] M. Hjorth-Jensen, T. T. S. Kuo, and E. Osnes, Phys. Rep. **261**, 125 (1995).
[33] E. Caurier and F. Nowacki, Act. Phys. Pol. **B30**, 705 (1999).
[34] E. Caurier et al., Rev. Mod. Phys. **77**, 427 (2005).
[35] R. du Rietz et al., Phys. Rev. Lett. **93**, 222501 (2004).
[36] R. Hoischen et al., J. Phys. G **38**, 035104 (2011).
[37] T. Baugher et al., Phys. Rev. **C 86**, 011305(R) (2012).
[38] A. Bohr and B. R. Mottelson, Nuclear Structure, Vol. 2, (Benjamin New York) (1975).
[39] M. Dufour and A. P. Zuker, Phys. Rev. **C 54**, 1641 (1996).
[40] T. Otsuka , M. Honma, and T. Mizusaki, Phys. Rev. Lett. **81**, 1588 (1998).
[41] A. Poves, Proc. 6th Int. Spring Seminar on Nucl. Phys.- Highlights of Modern Nuclear Structure,A.Covello (Ed.) World Scientific, Singapore , 193 (1999).
[42] D. C. Radford et al., Nucl. Phys. **A752**, 264c (2005).
[43] J. Terasaki , J. Engel, W. Nazarewicz, and M. Stoitsov, Phys. Rev. C **66**, 054313 (2002).
[44] http://www.nndc.bnl.gov/ensdf/, (2012).
[45] P. Doornenbal et al., Phys. Rev. C **78**, 031303 (2008).